CHEMISTRY
A EUROPEAN JOURNAL

DOI: 10.1002/chem.200801812

Size- and Distance-Dependent Nanoparticle Surface-Energy Transfer (NSET) Method for Selective Sensing of Hepatitis C Virus RNA

Jelani Griffin, Anant Kumar Singh, Dulal Senapati, Patsy Rhodes, Kanieshia Mitchell, Brianica Robinson, Eugene Yu, and Paresh Chandra Ray*[a]

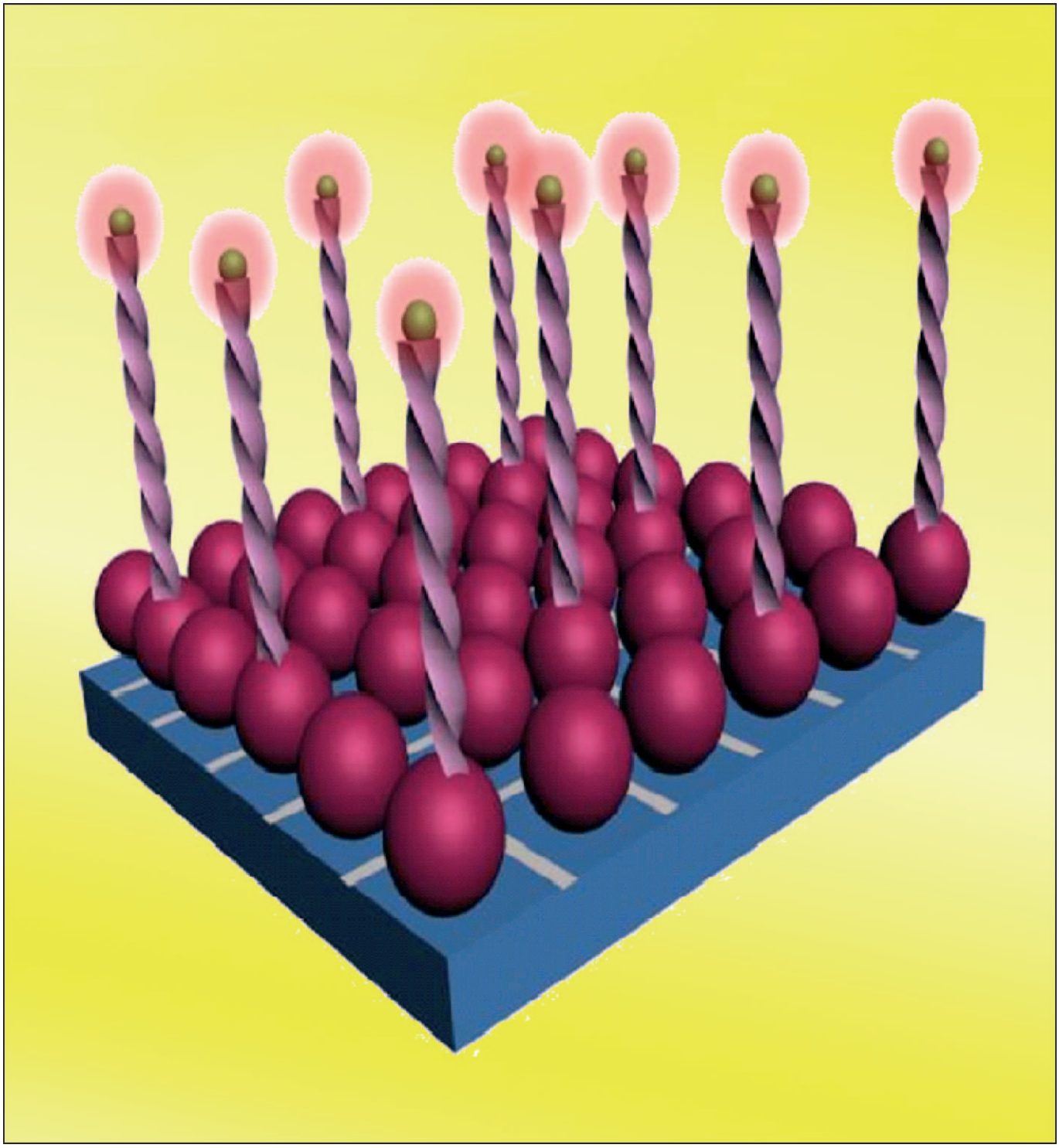

Abstract: We report size- and distance-dependent surface-energy transfer (SET) properties of gold nanoparticles for recognizing hepatitis C virus (HCV) RNA sequence sensitively and selectively (single-base mutations) in a homogeneous format. We have demonstrated that quenching efficiency increases by three orders of magnitude, as the particle size increases from 5 to 70 nm. Due to this extraordinarily high K_{SV}, nanoparticle SET (NSET) detection limit can be as low as 300 fM concentration of RNA, depending on the size of gold nanoparticle. We have shown that the distance-dependent quenching efficiency is highly dependent on the particle size and the distance at which the energy-transfer efficiency is 50%, ranges all the way from 8 nm, which is very close to the accessible distance of conventional Förster resonance energy transfer (FRET), to about 40 nm by choosing gold nanoparticles of different diameters. Our result points out that dipole-to-metal-particle energy transfer and NSET models provide a better description of the distance dependence of the quenching efficiencies for 8 nm gold nanoparticle, but agreement is poor for 40 and 70 nm gold nanoparticles, for which the measured values were always larger than the predicted ones.

Keywords: gold · nanostructures · RNA · surface-energy transfer

Introduction

The human suffering exacted by the hepatitis C virus is enormous. Hundreds of thousands of people die each year from liver failure and cancer caused by this infection. The hepatitis C virus (HCV) is a single-stranded RNA virus, which is responsible for chronic liver diseases, such as cirrhosis, end-stage liver disease, and hepatocellular carcinoma.[1–5] At present, the most widely used method of diagnosing HCV is the detection of anti-HCV antibodies using a screening enzyme-linked immunosorbent assay (ELISA), based on recombinant proteins from the HCV genome.[1–6] While it is highly sensitive and specific, this assay has huge limitations. For example, it cannot detect viruses during the early stage of infection, at a time when antibodies against HCV antigens are not produced. In addition, patients who are immuno-suppressed following transplantation, or who are immuno-compromised secondary to infection with the human immunodeficiency virus (HIV), may have the HCV infection, but without having any detectable antibodies. There is a need for a direct RNA-based test, which detects the presence of the HCV viral sequence. Recently reverse-transcriptase (RT)-polymerase chain reaction (PCR) method has been used to amplify and detect HCV RNA.[7,8] Although these approaches are convenient and provide low detection limits, these methods are time-consuming, laborious, and they lack the procedural simplicity for on-site analysis. The nanoscience revolution that sprouted throughout the 1990s is having a great impact on current and future RNA/DNA detection technology around the world.[9–41] The increasing availability of nanostructures with highly controlled optical properties in the nanometer size range has created widespread interest in their use in biotechnological system for diagnostic application and biological imaging.[9–41] Driven by the need, in this article we report ultra-sensitive nanoparticle surface-energy transfer (NSET) probe, based on gold nanoparticles, for screening of the hepatitis C virus (HCV) with excellent sensitivity and selectivity.

Recently, there have been many reports on the development of fluorescence-based assays for HCV RNA detection.[42,43] These assays are based on Förster resonance energy transfer (FRET)[44] or non-FRET quenching mechanisms. FRET is a spectroscopic technique for measuring distances in the 3–8 nm range.[45] Excitation energy of the donor is transferred to an acceptor through an induced-dipole/induced-dipole interaction. The efficiency of energy transfer (E) is given by $[1+(R/R_0)^6]^{-1}$ in which R is the distance between the donor and an acceptor and R_0 is the distance at which 50% of the energy is transferred and is a function of the spectral overlap of the donor emission and acceptor absorption, refractive index of the medium, quantum yield of the donor, and a factor κ^2 that depends on the relative orientation in space between the transition dipoles of donor and acceptor. Although FRET technology is very convenient and can be applied routinely at the single-molecule detection limit, the efficiency of FRET is very sensitive to the distance between the donor and an acceptor. The length scale for detection with the FRET-based method is limited by the nature of the dipole–dipole mechanism, which effectively constrains the length scales to distances on the order of <100 Å ($R_0 \approx 60$ Å) and FRET is observed when the donor and an acceptor are placed 20 bases apart on an oligonucleotide. The limitations of FRET can be overcome with a dynamic molecular method based on the distance-dependent plasmon coupling of metal nanoparticles. Recently several groups including ours[14,18–28,35–41] have reported that nanoparticle surface-energy transfer (NSET) is a technique capable of measuring distances nearly twice as far as FRET in which energy transfer from a donor molecule to a nanoparticle surface follows a predictable distance dependence. Like FRET,[44,45] the interaction for NSET is dipole–dipole in nature, but is geometrically different be-

[a] J. Griffin, Dr. A. K. Singh, Dr. D. Senapati, P. Rhodes, K. Mitchell, B. Robinson, E. Yu, Dr. P. C. Ray
Department of Chemistry
Jackson State University, Jackson, MS (USA)
Fax: (+1) 601-979-3674
E-mail: paresh.c.ray@jsums.edu

cause an acceptor nanoparticle has a surface and an isotropic distribution of dipole vectors to accept energy from the donor.[18--22,24,34–36,38] This arrangement increases the probability of energy transfer and accounts for the enhanced efficiency of NSET over FRET. In the case of resonant surface-plasmon excitation, a small dipole in the excited fluorophore induces a large dipole in the particle, leading to an enhancement in the energy-transfer efficiencies.[18–22,24,34–36,38] In this article, we present size and distance-dependent NSET properties of gold nanoparticles for recognizing HCV RNA sequence selectively (single-base mutations) in a homogeneous format.

Experimental Section

Hydrogen tetrachloroaurate ($HAuCl_4 \cdot 3H_2O$), $NaBH_4$, buffer solution, NaCl, and sodium citrate were purchased from Sigma–Aldrich and used without further purification. The HCV genome RNAs with different number of bases for example, RNA, 5′-(Cy3) UGUACUCACCG-GUUCCGCAGACCAC –3′, labeled with a Cy3 dye on the 5′-end, its complementary strand, complementary RNA with one base-pair mismatch and noncomplementary RNA strand, were purchased from Midland Certified Reagent (Midland, TX). These RNAs came as HPLC purified and were used without further purification.

Gold nanoparticle synthesis: Gold nanoparticles of 15 nm or above diameters were synthesized using reported method.[15–28] Gold nanoparticles of different sizes and shapes were synthesized by controlling the ratio of $HAuCl_4 \cdot 3H_2O$ and sodium citrate concentration as we reported recently.[15–22] For smaller gold nanoparticles, we used a sodium borohydride method as reported before.[15–21] $HAuCl_4 \cdot 3H_2O$ (0.01 M, 0.5 mL) in water and sodium citrate (0.01 M, 0.5 mL) in water were added to deionized H_2O (18 mL) and stirred. Next, an aqueous solution of freshly prepared 0.1 M $NaBH_4$ (0.1 M, 0.5 mL) was added and the solution changed from colorless to orange. Stirring was stopped and the solution was left undisturbed for 2 h. The resulting spherical gold nanoparticles were 4 nm in diameter. Transmission electron microscopy (TEM), UV/Vis absorption spectra, and colorimetric observation were used to characterize the nanoparticles (as shown in Figure 1). The particle concentration was measured by UV/Vis spectroscopy by using the molar extinction coefficients at the wavelength of the maximum absorption of each gold colloid as reported recently [$\varepsilon_{(15)518\,nm} = 3.6 \times 10^8\ cm^{-1}M^{-1}$, $\varepsilon_{(30)530\,nm} = 3.0 \times 10^9\ cm^{-1}M^{-1}$, $\varepsilon_{(40)533\,nm} = 6.7 \times 10^9\ cm^{-1}M^{-1}$, $\varepsilon_{(50)535\,nm} = 1.5 \times 10^{10}\ cm^{-1}M^{-1}$, $\varepsilon_{(60)540\,nm} = 2.9 \times 10^{10}\ cm^{-1}M^{-1}$, and $\varepsilon_{(80)550\,nm} = 6.9 \times 10^{10}\ cm^{-1}M^{-1}$].[15–22]

Preparation of gold nanoparticle adsorbed RNA probes: Probe RNA was incubated with gold particles for about 2 h at a ratio of 10 to 12 RNA molecules per particle. This ratio was used to ensure that each particle was conjugated to at least few RNA molecules. The RNA–gold nanoparticle conjugates were gradually exposed to NaCl (0.1 M) in a PBS buffer over a 1 h period, according to a procedure reported by us.[16,17,20,21] Since the ss-RNA is sufficiently flexible to partially uncoil its bases, they can be exposed to the gold nanoparticles. Under these conditions, the negative charge on the backbone is sufficiently distant so that attractive van der Waals forces between the bases and the gold nanoparticle are sufficient to cause ss-RNA to adsorb to the gold. Unadsorbed RNA probes were removed from the solution by centrifugation at 12000 rpm for 20 min. The final product was a red precipitate, which was resuspended and stored in 10 mM phosphate buffer.

Hybridization assays: A trial hybridization was performed by using 1:5 ratio of probe to target sequences in a phosphate buffer solution (PBS; 10 mM) containing NaCl (0.3 M). To break any secondary structure in the RNA target and allow hybridization with the probe, the trial solution was heated to 95 °C for 3 min and then cooled to an appropriate temperature for the desired assay for 1 min. The temperature for the hybridization experiment for simple sequence detection was typically ambient, while single-base-mismatch detection was performed at a temperature between the melting temperature of the mismatch and that of the perfect match.

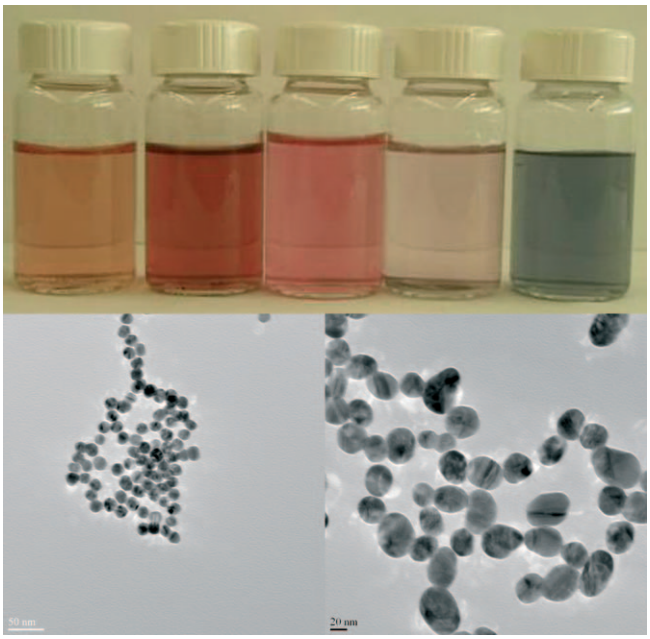

Figure 1. Top: Photographic image of (from left to right) 8, 20, 45, 70, and 110 nm gold nanoparticle solution. Bottom: TEM image of 8 nm (left, scale bar 50 nm) and 45 nm (right, scale bar 20 nm) gold nanoparticles.

NSET experimental setup: For fluorescence excitation, we used a continuous wavelength Melles–Griot green laser pointer (18 Lab 181) operating at 532 nm, as an excitation light source. Excitation light source was first attenuated using appropriate neutral density (ND) filter and coupled to the excitation arm of the Y-shaped reflection probe through a plano-convex lens (*f*:4.5 mm). Details of this portable sensing system have been reported recently.[18–20] A typical laser energy at the sample was adjusted to ≈1.3 mW with 0.3 ND filter. The fluorescence signal from sample was simultaneously collected by a ring of six optical fibers around the single illumination channel, in the backward direction (180° collection geometry). The collected emission signal was transmitted through an online filter module (containing a 570 nm cut-off filter to suppress the detection of the back-scattered excitation light) to a 600 μm core diameter UV grade fused silica auxiliary fiber prior to feeding it to the spectrometer. We used 200 μm illumination fiber and 50 μm read fiber. The collected laser-induced fluorescence (LIF) signal was fed into highly sensitive ocean optics OOI spectrometer. The emission spectrum was collected with Ocean Optics data acquisition software. All measurements performed with 5 ms integration time were instantaneously averaged with 5 spectra using the software. The averaged data were processed using Microsoft Excel program.

Results and Discussion

Size-dependent quenching properties: As shown in Figure 2, we observed a very distinct emission intensity change from fluorophore-tagged ss-RNA adsorbed on the gold nanoparticle. When a dye-labeled oligonucleotide molecule is adsorbed onto a nanoparticle, the fluorophore at the distal end can loop back and adsorb on the same particle (as shown in Scheme 1). Our experimental data showed a quenching effi-

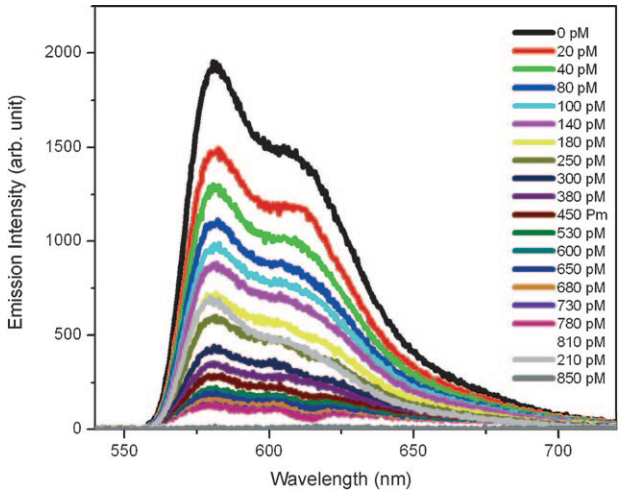

Figure 2. The quenching behavior of 450 nM 5′-(Cy3) UGUACUCACCGGUUCCGCAGACCAC3′ –3′ RNA as a function of 45 nm gold nanoparticle concentration (0 to 850 pM).

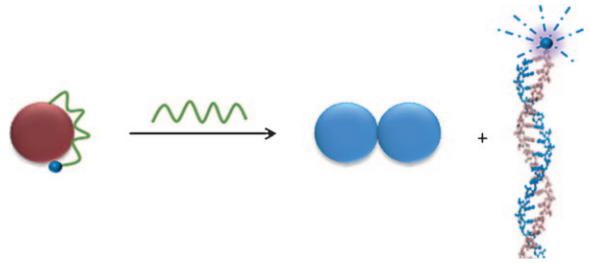

Scheme 1. Schematic representation of the RNA hybridization process, when RNA is adsorbed on gold nanoparticle.

ciency of nearly 98% when the fluorophore was statically adsorbed on the particle (static quenching).

Since the backbone of a single-stranded RNA is conformationally flexible, a favorable conformation for the adsorbed oligos would be an arch-like structure, in which both the 3′- and 5′-ends are attached to the particle but the RNA chain does not contact the surface.

Molecular chromophores situated in the vicinity of isolated colloidal metal particles in suspension usually experience quenching of their fluorescence, whereas photoluminescence may be enhanced in more complex structures that arise from the deposition of aggregated metal particles onto surfaces. The local field enhancement leads to an increased excitation rate, whereas nonradiative energy transfer to the particle leads to decrease of the quantum yield (quenching). Because of these competing effects, experiments showed either fluorescence enhancement or fluorescence quenching depending on the distance regime. The net luminescence can either decrease or increase depending on how the gold particle affects the chromophore's excitation rate R_{exc}, and the radiative and nonradiative decay rates of its excited state, R_{rad} and R_{nonrad}, which together determine the observed luminescence emission rate R_{emiss}.[14,18–28,46–48]

Figure 2 demonstrates the quenching behavior of 5′-Cy3-modified 5′-(Cy3) UGUACUCACCGGUUCCGCAGACCAC′ –3′ RNA as a function of 45 nm gold nanoparticle concentration ($\approx 10^{-11}$ M). The Stern–Volmer relationship[47] between quencher concentration and fluorescence intensity is given by Equation (1) in which ϕ_0 and F_0 are quantum yield and emission intensity in the absence of quencher, respectively; ϕ and F are the same parameters in the presence of quencher; k_q, k_e, and k_d are the rates of quenching, emission, and deactivation, respectively; K_{SV} is the Stern–Volmer quenching constant for collisional deactivation; and C_Q is the concentration of nanoparticle quencher.

$$\frac{\phi_0}{\phi} = \frac{F_0}{F} = 1 + \left(\frac{k_q}{k_e + k_d}\right)[C_Q] = 1 + K_{SV}[C_Q] \quad (1)$$

Figure 3 (top) shows a linear, have $F_0/F = 1$ intercepts, and exhibit slopes of $K_{SV} \approx 2.7 \times 10^{10}\,M^{-1}$ expressing very high quenching efficiency of the fluorophore excited state. Our results indicate that gold nanoparticle of 45 nm is 7–8 orders of magnitude more efficient than typical small-molecule dye–quencher pairs.[45] Figure 3 (bottom) shows how the

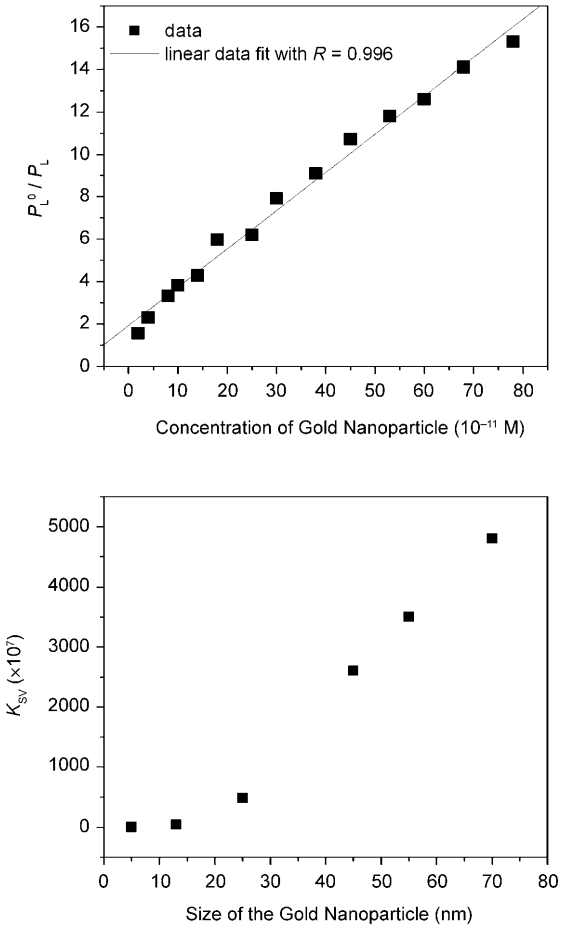

Figure 3. Top: Stern–Volmer plots of emission intensity change due to photoluminescence quenching by 45 nm gold nanoparticles. Bottom: Variation of Stern–Volmer Quenching Constant (K_{SV}) with gold nanoparticle size.

Stern–Volmer quenching constant (K_{sv}) varies with particle size. We can see from the figure that the quenching efficiency increases with the increase in particle diameter. The K_{SV} parameter increases from 4×10^{7} to 5×10^{10}, three orders of magnitude, as the particle size increases from 5 to 70 nm. This increment of quenching efficiency with particle size can be due to several factors: 1) reduced surface area of smaller nanoparticles will limit the dye accommodation on the gold nanoparticles; 2) we note the difference in the extinction coefficients (from 8×10^{7} to 3.2×10^{10}) of visible absorption spectra of 5- to 70 nm gold nanoparticles; and 3) our data indicate increase in overlap between nanoparticle absorption with Cy3 emission with particle size. Due to this high K_{SV}, quenching can be observed even at subpicomolar concentrations of nanoparticles, suggesting that the combination of Cy3-modified DNA with the proper size of gold nanoparticles can potentially lead to highly sensitive optical biosensors.

Distance-dependent NSET: Although FRET technology is very convenient and can be applied routinely at the single-molecule detection limit, the length scale for detection by using Förster method is limited by the nature of the dipole–dipole mechanism. The quantum efficiency of energy transfer is given by Equation (2), in which R is the distance between donor and acceptor, R_0 is the distance between donor and acceptor at which the energy transfer efficiency is 50%.

$$\Phi_{EnT}=\frac{1}{1+\left(\frac{R}{R_0}\right)^{n}} \qquad (2)$$

In the case of Förster or dipole–dipole energy transfer, $n=6$ and $R_0\approx3$–8 nm for typical fluorophores.[45] To understand the limitation of our NSET probe in terms of length of RNA and size of gold nanoparticle, we have used HCV genome RNA of different lengths. Here we have used ss-RNA of different lengths attached to gold nanoparticles of different sizes by using thiol–gold chemistry (as shown in Scheme 2, top). For this purpose, −SH-linked RNAs were gradually exposed to gold nanoparticles in a PBS buffer over a 16 h period, according to a procedure reported by Mirkin and co-workers.[13] Unlike the previous experiments, in this case the RNA cannot come off the particles upon hybridization. Scheme 2 (bottom) shows a schematic diagram of the NSET probes and their operating principles for different length RNA. After hybridization, by varying the RNA lengths, the separation distance between gold nanoparticle and Cy3 dye can be systematically varied between 8 and 50 nm, by varying the number of base pairs. The distance from the center of the molecule to the metal surface is estimated by taking into account the size of the fluorescent dye, 0.32 nm for each base pair,[49,50] and 1.8 nm for Au–S distance and base-pair-to-dye distance. As a result, after hybridization the distance becomes 8.2 nm for 20 bp RNA, 14.6 nm for 40 bp RNA, 24.2 nm for 70 bp RNA, and 40.2 nm for 120 bp RNA. We have assumed a linear ds-RNA configuration, because ds-RNA is known to be rigid having a persistence length of 90 nm.[32]

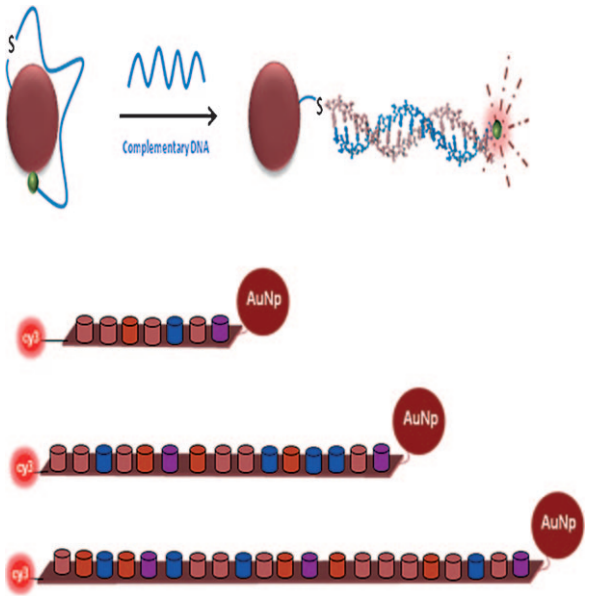

Scheme 2. Top: Schematic representation of the RNA hybridization process, when one end of the RNA is covalently coupled through thiol–gold chemistry. Bottom: Schematic illustration of 5′JOE and 3′-SH-modified DNA of different lengths

Figure 4 (top) shows how the quenching efficiency varies with the increase in the distance between gold nanoparticle and Cy3 dye for gold nanoparticles of different particle size. Figure 4 (bottom) shows how R_0 (distance at which the energy transfer efficiency is 50%) value varies with the size of gold nanoparticles. Our results indicate that one can tune R_0 ranging all the way from 8 nm, which is very near to the accessible distance of conventional FRET (6 nm), to about 40 nm by choosing gold nanoparticles of different diameters.

To understand the distant-dependent quenching process, we tried to fit our data (as shown in Figure 5) with theoretical modeling by using general FRET and dipole-to-NSET employed by Jeening et al.[22] Our results indicate that the long-distance quenching rate is better described with a slower distance-dependent quenching rate than the classical $1/R^6$ characteristic of Förster energy transfer. Our results also point out that NSET model provides a better description of the distance dependence of the quenching efficiencies for 8 nm gold nanoparticle (as shown in Figure 5, top), but agreement is very poor for 40 and 70 nm gold nanoparticles (as shown in Figure 5 middle and bottom), for which the measured values were always larger than the predicted ones. We also tried to fit our data with dipole-to-metal-particle energy transfer (DMPET) model as used by Pons et al.,[36] but in this case there is only good agreement with experimental data for the 8 nm gold nanoparticle. Although in general the interactions between nanoparticle and dye are quite complex when considering all illumination polarizations, distance ranges, and particle sizes, the situation can be understood as follows.

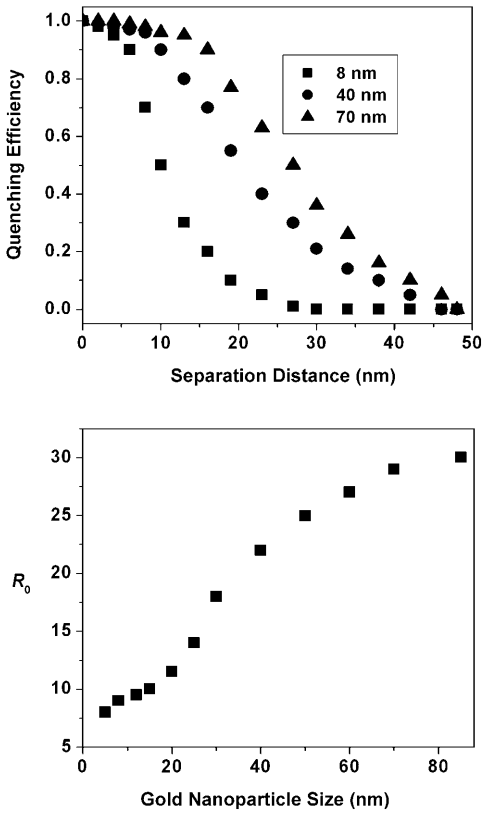

Figure 4. Top: Variation of the quenching efficiency with distance between gold nanoparticle and Cy3 dye. Bottom: Variation of R_0 with the size of gold nanoparticle.

1) Since FRET physically originates from the weak electromagnetic coupling of two dipoles, one can imagine that introducing additional dipoles and thus providing more coupling interactions can circumvent the FRET limit. Light induces oscillating dipole moments in each gold particle, and their instantaneous $(1/r)^3$ coupling results in a repulsive or attractive interaction, modifying the plasmon resonance of the system. The softer dependence of the interaction strength on particle separation r results in a much longer interaction range compared to general FRET.
2) The fluorescence quantum yield is determined by the radiative rate constant, k_r, and its nonradiative counterpart, k_{nr}: $\tau=(k_r+k_{nr})^{-1}$. At small distances (1–2 nm), the large fluorescence quenching efficiency of 99.8% is due to two effects: a) gold nanoparticles increase the nonradiative rate R_{nonrad} of the molecules due to energy transfer; b) the radiative rate R_{rad} of the molecules decreases because the molecular dipole and the dipole induced on the gold nanoparticles radiate out of phase if the molecules are oriented tangentially to the gold nanoparticle's surface. At higher distance, the distance dependent quantum efficiency is almost exclusively governed by the radiative rate as reported recently by Seelig et al.[35] They found that nanoparticle-induced lifetime modification can serve as a nanoscopic technique for the distance

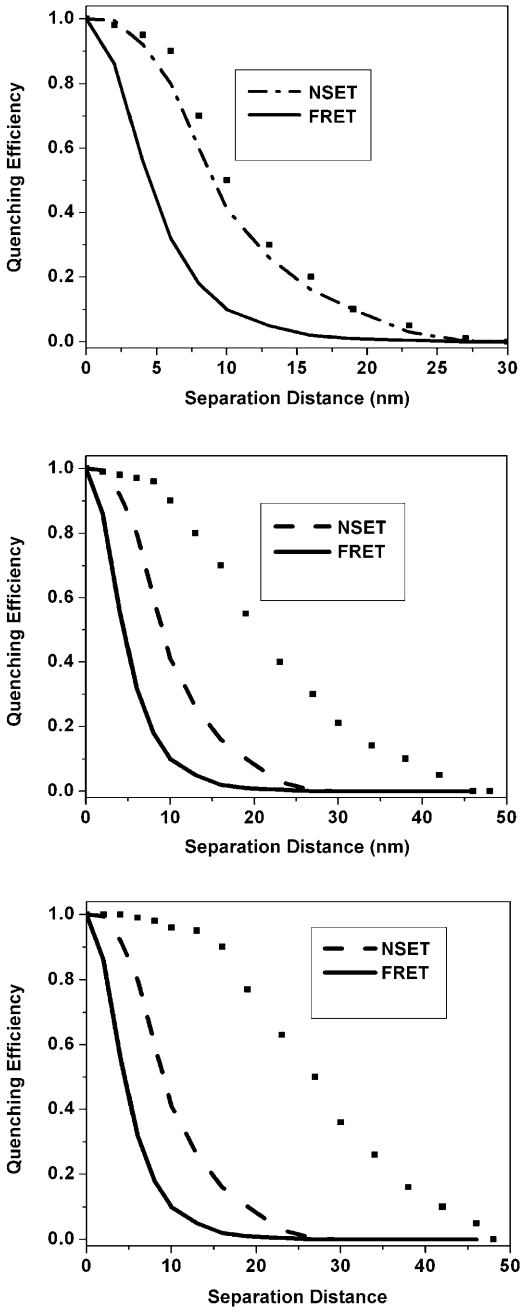

Figure 5. Fitting of data of variation of the quenching efficiency with distance using FRET, NSET theoretical model and experimental values for 8 nm (top), 40 nm (middle), and 70 nm (bottom) gold nanoparticles.

range well beyond 10 nm, which is the upper limit of FRET. Their result shows that the lifetime (τ_r) highly depends on the particle size as well as the distance between nanoparticle and dyes. Their data indicate that for bigger size nanoparticle (20–40 nm in diameters), τ_r is highly sensitive with small changes in the dye–particle distance even if they are separated by up to 40 nm, which explains our observation of high variation of R_0 with gold nanoparticle size.

Our observations also indicate that when one chooses the experimental parameters for optimizing the NSET sensitivity, it is very important to take into account the effect of the gold nanoparticle size, which strongly affects the quenching efficiency and distance-dependent NSET. One has to remember that due to the effect of surface charge, surface coverage, and mutual strand interaction on the bending properties of individual RNA strand, the apparent length of the oligonucleotides can be smaller than their expected molecular length.

RNA hybridization detection: Scheme 1 shows a schematic diagram of the nanoparticle probes and their operating principles for single RNA hybridization detection process. Upon target binding, due to the duplex structure, the double-strand (ds) RNA does not adsorb onto gold and the fluorescence persists. This structural change generates a fluorescence signal that is highly sensitive and specific to the target RNA. In this case, instead of covalently binding the probe-RNA to the gold nanoparticle, as we used for understanding the distant dependent NSET process, the probe-RNA is reversibly adsorbed to the gold nanoparticle. Thus, upon hybridization of the target-RNA, the resultant ds-RNA is completely released into the solution instead of being left tethered to the gold particle. There are several advantages in this adsorption method over covalent linking method and these are as follows:

1) The covalent binding process between gold nanoparticle and RNA is very time consuming and takes about two days, whereas the adsorption of RNA on gold nanoparticles occurs within an hour.
2) As we have shown in Figure 4 (top), the quenching efficiency is above 95% even for distance at 4 nm. So in case of covalent binding system, since after hybridization, the distance between dye and gold nanoparticle is less than 4 nm for RNA with less than 10 base pairs, one cannot use gold-nanoparticle-based NSET method to detect RNA hybridization for RNAs having 2–10 base pairs. On the other hand, the nonlinking system that we have used here can be conveniently used for shorter RNA systems (2–10 base pairs).
3) In the linking system, the aggregation process is slower than that of the nonlinking system, as we and others reported before.[16,20,52–54]

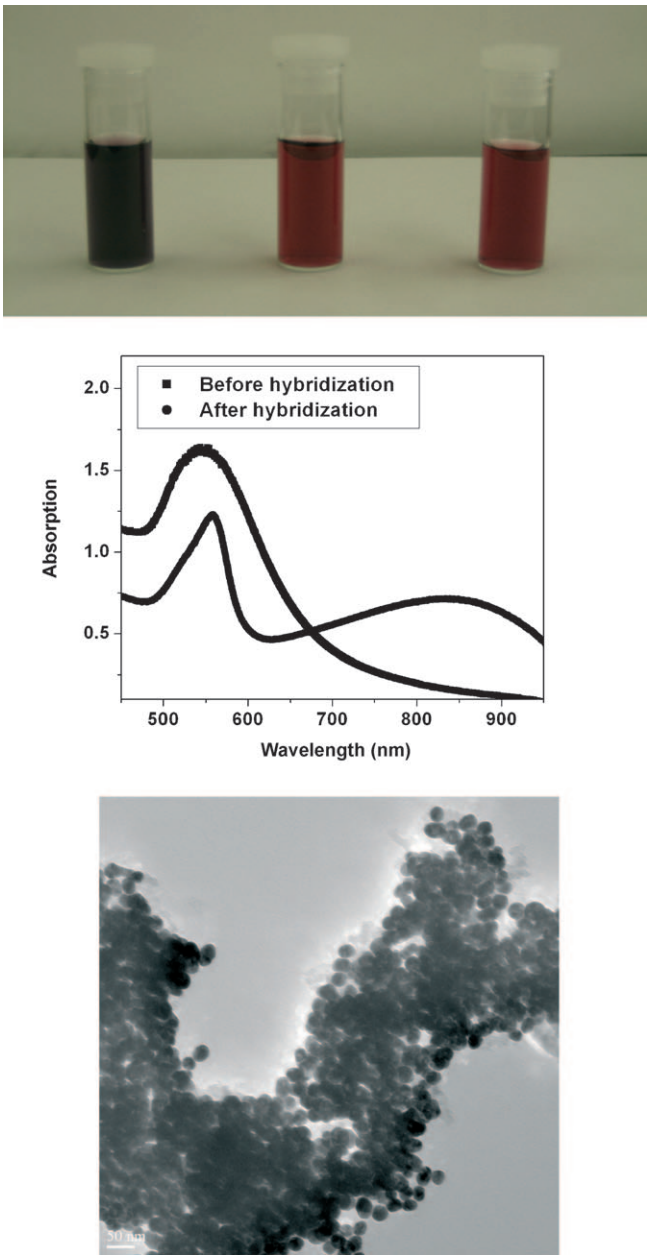

Figure 6. Top: Photograph showing colorimetric change upon addition of exact complementary RNA (left), complementary RNA with one base-pair mismatch (middle) and noncomplementary RNA (right). Middle: Absorption spectral change before and after hybridization. Bottom: TEM image showing aggregation after hybridization (scale bar 50 nm).

When target RNA with complementary sequence is added to the probe RNA, a clear colorimetric change from red to blue-gray is observed within few minutes (as shown in Figure 6, top) and we noted the plasmon band shifted from 512 to 750 nm (as shown in Figure 6, middle). Figure 6 (bottom) shows the TEM image after hybridization and our results indicate that gold nanoparticles undergo aggregation after hybridization, owing to the presence of sodium chloride. Gold nanoparticles in solution are typically stabilized by adsorbed negative citrate ions whose repulsion prevents the strong van der Waals attraction between gold particles from causing them to aggregate. As soon as the ds-RNA separated from the gold nanoparticle, aggregation of gold nanoparticle occurs. This is due to the screening effect of the salt, which minimizes electrostatic repulsion between the nanoparticles. Our zeta potential measurement using Zetasizer NanoZS shows that negatively charged surface (zeta potential −63.5 mV) of the nanoparticles reduced surface charge (zeta potential −9.8 mV) in presence of 0.08 M NaCl. So after hybridization, due to presence of around 0.4 M NaCl, screening effect of salt leads to more linked particles

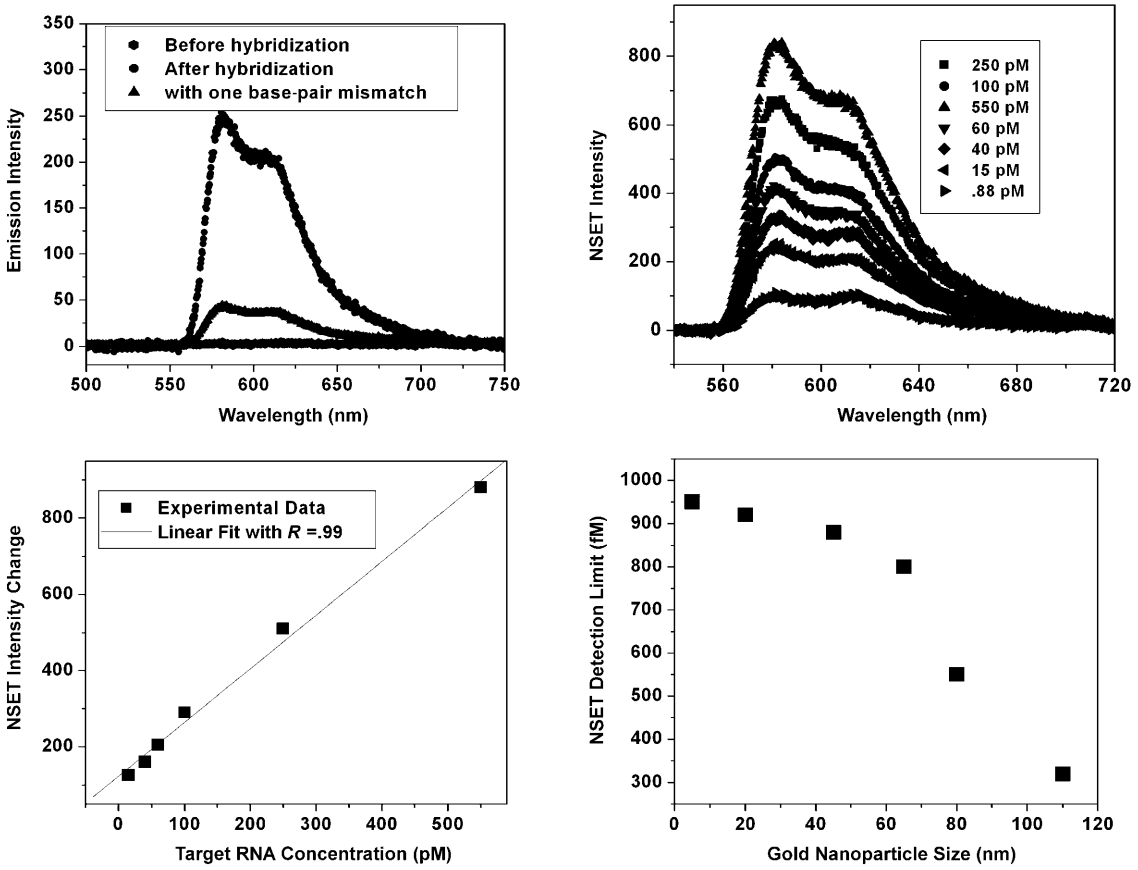

Figure 7. Top left: Plot of fluorescence intensity versus wavelength for 40 pM 5′-Cy3-modified HCV RNA (Cy3–5′UGUACUCACCGGUUCCGCA-GACCAC-3′) adsorbed onto 45 nM gold nanoparticles before hybridization; after hybridization with complementary RNA, which has one base-pair mismatch at the end; and after hybridization with exact complementary RNA. Top right: Fluorescence response upon addition different concentration of target RNA on 150 nm probe RNA. Bottom left: Plot of fluorescence intensity vs. target RNA concentration in pM. Linear correlation exists over the range of 15–550 pM with $R = 0.994$. Bottom right: Variation of NSET sensitivity with gold nanoparticle size.

and hence larger damping of the surface plasmon absorption of Au nanoparticle surfaces. This structural change generates a fluorescence signal that is highly sensitive and specific to the target RNA.

As shown in Figure 7 (top, left), we observed a very distinct NSET intensity change after hybridization even at 120 pM concentration of probe fluorophore-tagged ss-RNA. Since the surface adsorption energies of organic dyes on gold are usually in the range of 8–16 kcal mol^{-1}, which are much smaller than the energies involved in RNA hybridization (80–100 kcal mol^{-1}), after hybridization the constrained conformation is opened and the fluorophore is separated from the particle surface. This high fluorescence enhancement clearly demonstrates that nanoparticle-based SET assay can be used as a highly sensitive probe for monitoring RNA hybridization. Figure 7 (top, left) also illustrates single-mismatch detection capability. Our result indicates that our NSET probes are highly specific in discriminating against noncomplementary RNA sequences and single-base mismatches. The addition of noncomplementary nucleic acids had no effect on the fluorescence, and a single-base mismatch reduced the fluorescence intensity by 90% (in comparison with the fluorescence intensity of perfectly matched targets). So our NSET probes will be applicable for rapid detection of single-nucleotide polymorphisms (SNPs) in genomic RNA, an exciting prospect for eliminating time-consuming and expensive gel-sequencing procedures that are currently the standard protocol.

Size-dependent sensitivity and quantitative measurement of sequence specific target DNA concentration: To evaluate whether our NSET probe is capable of measuring target RNA concentration quantitatively, we performed NSET intensity measurement at different concentrations of target RNA. As shown in Figure 7 (top, right), the NSET emission intensity is highly sensitive to the concentration of target RNA and the intensity increased linearly with concentration. Our data indicate that NSET with 45 nm gold nanoparticles, exhibits sensitivity to detect RNA as low as 880 fM. Linear correlation was found between the emission intensity and the concentration of target RNA over the range of 15–550 pM (as shown in Figure 7 bottom, left). So our NSET probe can provide a quantitative measurement of HCV genome RNA concentration in a sample. Figure 7 (bottom, right) shows how the NSET detection limit for HCV 25 bases RNA detection varies with particle size. The detection

limits for NSET such that the NSET intensity change is 12, before and after hybridization. As we can note from the figure, NSET sensitivity highly depends on the particle diameter. As the particle diameter increases, the detection limit becomes better and better and our data indicate that NSET can detect RNA as low as 300 fM, when the particle size is 110 nm. This variation of sensitivity efficiency with particle size can be due to several factors: 1) reduced surface area of smaller nanoparticles will limit the dye-tagged RNA accommodation on the gold nanoparticles and 2) increasing overlap between nanoparticle absorption with Cy3 emission and K_{SV} values with increasing particle size. So our experimental data suggests that the combination of Cy3-modified RNA with the proper size of gold nanoparticles can potentially lead to highly sensitive optical biosensors.

Conclusion

In conclusion, in this manuscript we have reported ultra-sensitive gold-nanoparticle-based SET for screening of the hepatitis C virus (HCV) RNA, with excellent sensitivity (800 fM) and selectivity (single-base-pair mismatch). We have shown the particle size-dependent super-quenching properties of gold nanoparticles with Stern–Volmer constants approaching $10^{11}\,M^{-1}$, 7–8 orders of magnitude higher than the small-molecule dye–quencher pairs. Our experiment indicate that the quenching efficiency increases by three orders of magnitude, as the particle size increases from 5 to 70 nm. Due to this extraordinarily high K_{SV}, quenching can be observed even at subpicomolar concentrations of the Cy3 dye-tagged RNA oligomers, suggesting that the combination of Cy3-modified RNA with these gold nanoparticles of appropriate size can be potentially used as highly sensitive optical biosensor. Linear correlation was found between the emission intensity and concentration of the target RNA over the range of 15–550 pM, which indicates that the NSET probe can provide a quantitative measurement of HCV RNA concentration. The NSET size detection limit indicates that NSET sensitivity is highly dependent on the particle size. Our observation indicates that the distance-dependent quenching efficiency is highly dependent on the particle size. We show that we can tune R_0 (distance at which the energy transfer efficiency is 50%) ranging all the way from 8 nm, which is very near to the accessible distance conventional FRET (6 nm), to about 40 nm by choosing gold nanoparticles of different diameters. The long-distance quenching rate is better described with a slower distance-dependent quenching rate than the classical $1/R^6$ characteristic of Forster energy transfer. In addition the DMPET and NSET models provide a better description of the distance dependence of the quenching efficiencies for 8 nm gold nanoparticles, but agreement is poor for 40 and 70 nm gold nanoparticles, for which the measured values were always larger than the predicted ones. This distance-dependence phenomenon can be engineered by choosing the size of the nanoparticle and serves as a nanoscopic method for measuring distances beyond that which is accessible to FRET. By designing more efficient optical nanoantennas and tailoring their plasmon resonances, one could considerably enhance the sensitivity of this method. Looking into the future, we expect that these sensor developments will have important implications in the development of better biosensors and bioassay for application to clinical analysis and biomedical research. Continued optimization of different parameters is necessary to determine the applicability of these assays in point-of-care settings. The ability of an assay to detect RNA in complex environments with high background and competing targets requires exquisite selectivity and sensitivity and will ultimately serve as a yardstick for determining its applicability in real environmental settings.

Acknowledgement

Dr. Ray thanks NSF-BIO grant #0641455, NSF-PREM grant #DMR-0611539 for their generous funding. We also thank the reviewer whose valuable suggestions improved the quality of manuscript.

[1] C. L. Jopling, M. K Yi, A. M. Lancaster, S. M. Lemon, P Sarnow, *Science* **2005**, *309*, 1577.
[2] X. Zhang, G. C. Segers, Q. Sun, F. Deng, D. L. Nuss, *J. Virol.* **2008**, *82*, 2613.
[3] B. R. Cullen, *Science* **2007**, *317*, 329.
[4] A. G. Cairns-Smith, *Chem. Eur. J.* **2008**, *14*, 3830.
[5] J. R. Thomas, P. J. Hergenrother, *Chem. Rev.* **2008**, *108*, 1171.
[6] T. T. Saxowsky, P. W. Doetsch, *Chem. Rev.* **2006**, *106*, 474.
[7] Y. Tang, H. Li, A. Roberto, D. Warner, B. Yen-Lieberman, *J. Clin. Virol.* **2003**, *31*, 148.
[8] W. N. Schmidt, D. Klinzman, D. R. Labrecque, D. E. Macfarlane, J. T. Stapleton, *J. Med. Virol.* **2005**, *47*, 153.
[9] S. K. Ghosh, T. Pal, *Chem. Rev.* **2007**, *107*, 4797.
[10] A. P. Alivisatos, *Nat. Biotechnol.* **2004**, *22*, 47.
[11] E. Katz, I. Willner, *Angew. Chem.* **2004**, *116*, 6166; *Angew. Chem. Int. Ed.* **2004**, *43*, 6042.
[12] J. Xiang, W. Lu, Y. Hu, Y. Wu, H. Yan, C. M. Lieber, *Nature* **2006**, *441*, 489.
[13] J. M. Nam, C. S. Thaxton, C. A. Mirkin, *Science* **2003**, *301*, 1884.
[14] G. Battistini, P. G. Cozzi, J. Jalkanen, M. Montalti, L. Prodi, N. Zaccheroni, F. Zerbetto, *ACS Nano* **2008**, *2*, 77.
[15] G. K. Darbha, A. K. Singh, U. S. Rai, E. Yu, H. Yu, P. C. Ray, *J. Am. Chem. Soc.* **2008**, *130*, 8038.
[16] G. K. Darbha, U. S. Rai, A. K. Singh, P. C. Ray, *Chem. Eur. J.* **2008**, *14*, 3896.
[17] P. C. Ray, *Angew. Chem.* **2006**, *118*, 2218; *Angew. Chem. Int. Ed.* **2006**, *45*, 1151.
[18] G. K. Darbha, A. Ray, P. C. Ray, *ACS Nano* **2007**, *1*, 208.
[19] V. S. Tiwari, T Oleg, G. K. Darbha, W. Hardy, J. P. Singh, P. C. Ray, *Chem. Phys. Lett.* **2007**, *446*, 77.
[20] P. C. Ray, G. K. Darbha, A. Ray, W. Hardy, *Nanotechnology* **2007**, *18*, 375504.
[21] P. C. Ray, A. Fortner, G. K. Darbha, *J. Phys. Chem. B* **2006**, *110*, 20745.
[22] T. L. Jennings, M. P. Singh, G. F. Strouse, *J. Am. Chem. Soc.* **2006**, *128*, 5462.
[23] B. Tang, L. Cao, K. Xu, L. Zhuo, J. Ge, Q. Li, L. Yu, C. P. Ray, *Chem. Eur. J.* **2008**, *14*, 3637.
[24] T. L. Jenning, J. C. Schlatterer, M. P. Singh, N. L. Greenbaum, G. F. Strouse, *Nano Lett.* **2006**, *6*, 131.
[25] L.-Q. Chu, R. Förch, W. Knoll, *Angew. Chem.* **2007**, *119*, 5032; *Angew. Chem. Int. Ed.* **2007**, *46*, 4944.

[26] T. N. Grossmann, L. Röglin, O. Seitz, *Angew. Chem.* **2007**, *119*, 5315; *Angew. Chem. Int. Ed.* **2007**, *46*, 5223.
[27] X. Huang, I. H. El-Sayed, W. Qian, M. A. El-Sayed, *J. Am. Chem. Soc.* **2006**, *128*, 2115.
[28] X. Huang, I. H. El-Sayed, W. Qian, M. A. El-Sayed, *Nano Lett.* **2007**, *7*, 1591.
[29] G. H. Chan, J. Zhao, E. M. Hicks, G. C. Schatz, R. P. Van Duyne, *Nano Lett.* **2007**, *7*, 1947.
[30] B. P. Khanal, E. R. Zubarev, *Angew. Chem.* **2007**, *119*, 2245; *Angew. Chem. Int. Ed.* **2007**, *46*, 2195.
[31] C.-C. Huang, Z. Yang, K.-H. Lee, H.-T. Chang, *Angew. Chem.* **2007**, *119*, 6948; *Angew. Chem. Int. Ed.* **2007**, *46*, 6824.
[32] L. Fabris, M. Dante, G. Braun, S. J. Lee, N. O. Reich, M. Moskovits, T.-Q. Nguyen, G. C. Bazan, *J. Am. Chem. Soc.* **2007**, *129*, 6086.
[33] S. Lal, N. K. Grady, G. P. Goodrich, N. J. Halas, *Nano Lett.* **2006**, *6*, 2338.
[34] N. J. Durr, T. Larson, D. K. Smith, B. A. Korgel, K. Sokolov, A. B-Yakar, *Nano Lett.* **2007**, *7*, 941.
[35] J. Seelig, K. Leslie, A. Renn, S. Kuhn, V. Jacobsen, M. van de Corput, C. Wyman, V. Sandoghdar, *Nano Lett.* **2007**, *7*, 685.
[36] T. Pons, I. L. Medintz, K. E. Sapsford, S. Higashiya, A. F. Grimes, D. S. English, H. Mattoussi, *Nano Lett.* **2007**, *7*, 3157.
[37] N. Abe, H. Abe, Y Ito, *J. Am. Chem. Soc.* **2007**, *129*, 15108.
[38] L. R. Skewis, B. M. Reinhard, *Nano Lett.* **2008**, *8*, 214.
[39] G. Battistini, P. G. Cozzi, J. Jalkanen, M. Montalti, L. Prodi, N. Zaccheroni, F. Zerbetto, *ACS Nano* **2008**, *2*, 77.
[40] B. Saccà, R. Meyer, U. Feldkamp, H. Schroeder, C. M. Niemeyer, *Angew. Chem.* **2008**, *120*, 2165; *Angew. Chem. Int. Ed.* **2008**, *47*, 2135.
[41] S. Lee, E.-J. Cha, K. Park, S.-Y. Lee, J.-K. Hong, I.-C. Sun, S. Y. Kim, K. Choi, I. C. Kwon, K. Kim, C.-H. Ahn, *Angew. Chem.* **2008**, *120*, 2846; *Angew. Chem. Int. Ed.* **2008**, *47*, 2804.
[42] M. Schroter, B. Zöllner, P. Schäfer, R. Laufs, H.-H. Feucht, *J. Clin. Microbiol.* **2001**, *39*, 765.
[43] J. Bartolomé, J. M. López-Alcorocho, I. Castillo, E. Rodríguez-Iñigo, J. A. Quiroga, R. Palacios, V. Carreño, *J. Virol.* **2007**, *81*, 7710.
[44] T. Förster, *Ann. Phys.* **1948**, *2*, 55.
[45] J. R. Lakowicz, *Principles of Fluorescence Spectroscopy*, Kluwer Academic/Plenum, New York, **1999**.
[46] R. Bose, J. F. McMillan, J. Gao, K. M. Rickey, C. J. Chen, D. V. Talapin, C. B. Murray, C. W. Wong, *Nano Lett.* **2008**, *8*, 2006.
[47] L. Wang, W. Tan, *Nano Lett.* **2006**, *6*, 84.
[48] B. Tang, L. Cao, K. Xu, L. Zhuo, J. Ge, Q. Li, Y. Guiwen, *Chem. Eur. J.* **2008**, *14*, 522.
[49] J. A. Schellman, *Biopolymers* **1974**, *13*, 217.
[50] C. Frontali, E. Dore, A. Ferranto, E. Gratton, A. Bettini, M. R. Pozzan, E. Valdevit, *Biopolymers* **1979**, *18*, 1353.
[51] H. Li, L. J. Rothberg, *Anal. Chem.* **2004**, *76*, 5414.
[52] K. Sato, K. Hosokawa, M. Mazeda, *Nucleic Acids Res.* **2005**, *33*, 4e.
[53] K. Sato, M. Onoguchi, Y. Sato, K. Hosokawa, M. Maeda, *Anal. Biochem.* **2006**, *350*, 162.
[54] H. X. Li, L. J. Rothberg, *Proc. Natl. Acad. Sci. USA* **2004**, *101*, 14036.

Received: September 3, 2008
Published online: November 26, 2008

